IEEE Access
Multidisciplinary | Rapid Review | Open Access Journal

Received January 6, 2021, accepted January 14, 2021, date of publication January 22, 2021, date of current version February 1, 2021.

Digital Object Identifier 10.1109/ACCESS.2021.3053654

Leader/Follower Force Control of Aerial Manipulators

KONSTANTINOS GKOUNTAS[1] AND ANTHONY TZES[2], (Senior Member, IEEE)
[1]Department of Electrical and Computer Engineering, University of Patras, 26500 Patras, Greece
[2]Program of Electrical and Computer Engineering, New York University Abu Dhabi, Abu Dhabi, United Arab Emirates

Corresponding author: Konstantinos Gkountas (gkountas@ece.upatras.gr)

This research is co-financed by Greece and the European Union (European Social Fund- ESF) through the Operational Programme ≪Human Resources Development, Education and Lifelong Learning≫ in the context of the project "Strengthening Human Resources Research Potential via Doctorate Research" (MIS-5000432), implemented by the State Scholarships Foundation (IKY).

ABSTRACT This article focuses on the modeling and controlling of Unmanned Aerial Manipulators (UAMs) in a leader/follower configuration performing a cooperative manipulation task. Each UAM consists of an Unmanned Aerial Vehicle (UAV) with an attached serial-link robotic manipulator. The Recursive Newton-Euler dynamics formulation is employed to account for the interaction between the UAV and its manipulator. The overall system consists of a couple UAMs with a carrying load. The coupling between these systems is due to the exerted forces by their manipulators through the object characterized by its stiffness matrix. A leader/follower control scheme is employed with a stability-analysis tailored to the UAM-pair. The leader UAM defines the trajectory of the moving object while the follower acts so as to reduce the system's internal reaction forces. Simulation studies are employed to validate the controller's performance while comparing the system's response against that derived from a classical nonlinear tracking controller.

INDEX TERMS Aerial manipulation, cooperation, control, manipulator, robotics, unmanned aerial systems.

I. INTRODUCTION

The adoption of Unmanned Aerial Vehicles (UAVs) has expanded the research applications in several fields, spanning from surveillance and filming to aerial manipulation, in which UAVs equipped with manipulators interact with the infrastructure. The UAVs' physical interaction with their environment has led to the funding of several projects [1]–[3] and many interesting studies on aerial manipulation [4].

In [5], a tiltrotor is used to generate a forward-pushing force to translate an obstacle. In [6], a UAV uses an elastic tool to interact with the objects positioned higher than the UAV's body, whereas in [7], a UAV cooperates with a ground robot in order to manipulate an object. In [8], the coupled model of a UAV with a manipulator is examined. The movement, though, of the manipulator significantly affects the aerial system's center of mass (CoM), and, thus, in [9], [10] parallel structure manipulators are used in order to minimize the reaction forces/torques and improve the overall stiffness. In [11], a new manipulation system is proposed where a continuum robotic arm is used for cluttered environments.

Aerial manipulators expand their range of applications by using grippers in their end-effector [12], [13]. A dual-arm aerial manipulator system grasps and turns a valve in [14], while dynamic controllers [15] are designed to improve the system's performance. A hexacopter and a 7-Degree of Freedom (DoF) manipulator are utilized to grasp a moving target in [16], while the effect of external disturbances is accounted in [17]. In [18], the authors developed a 5-DoF aerial manipulator for inspection by contact, which is enhanced with a rolling base for moving on a horizontal surface.

Rather than relying on a single Unmanned Aerial Manipulator (UAM), multiple aerial manipulators can cooperate to overcome the constraint of the payload limitation. In [19]–[24], a load is transferred with cables, while in [25], UAVs are tethered to an object, trying to manipulate it under environmental disturbances. In [26], multiple flying vehicles were used to carry a flexible payload, while in [27] an adaptive controller was used to calculate the inputs in each UAM to equally contribute to transport a point-mass load. In [28], several UAMs interact with their environment, using,

The associate editor coordinating the review of this manuscript and approving it for publication was Hassen Ouakad.

though, passive spherical joints for the manipulation. Passive spherical joints are used in their tethering method since this reduces the reaction torque caused by the load translation at the expense of precise maneuvering offered by a robotic manipulator.

In most cases, a centralized method is deployed to control the group of the aerial manipulators. Centralized methods demand all the state information of all subsystems, in order to send the appropriate commands to every aerial system. All the information has to travel back and forth, adding an extra delay in the controllers of the UAMs. Moreover, each new UAM that is going to contribute to the system's objective, adds communication burden, resulting in a nonscaleable system. However, in decentralized methods, each controller of the UAMs uses only its state vector and the information gathered by its sensors [29]. In [30], the authors proposed a decentralized controller for UAVs attached to an object given that each UAV knows its fixed relative position and orientation with respect to the transported item.

Unlike schemes that interact with a slung-load using a tethered configuration [19], [21], [31] which is equivalent of using moving spherical joints and a passive force control, or using sliding mode controllers for a UAV-pair on a two-dimensional plane [32], this article deals with the cooperation problem between two UAMs in a leader/follower formation while exercising forces and torques in an object carried by their manipulators, as shown in Fig. 1. These UAMs can be considered mechanically coupled, since there are reaction forces and torques transferred from their manipulators in a similar manner as in [30]. However our model-based controller relies on the complete dynamic model rather than assuming a rigidly attached aerial manipulator array. The interaction between the UAMs due to the carried object, instability can occur because of the transmitted forces/torques from the base of the manipulators to their UAV-base; the principle is bio-inspired [33], where the follower indirectly detects the forces that the leader exert on the object.

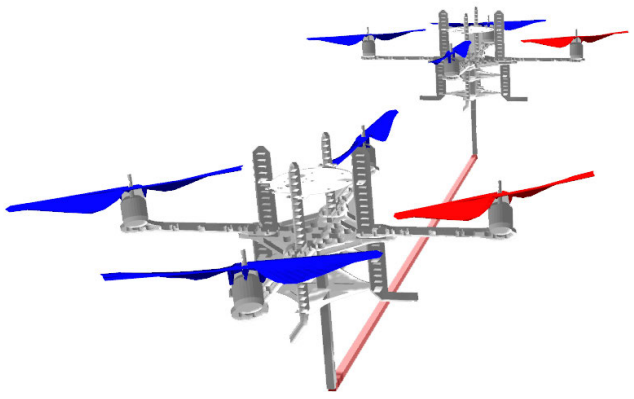

FIGURE 1. Cooperating UAMs carrying an object.

The purpose of this work is to derive the dynamic equations that describe two UAMs while they are cooperating for a load transportation. The equations should include, not only, the interaction between each UAM, but also the interaction in each UAV with its manipulator. Hence, the Recursive Newton-Euler (RNE) formulation is employed to compute the generalized forces from the tip of each manipulator to the base of UAV. Afterwards, the interconnection between these UAMs is achieved by the object's stiffness properties, that is used to compute the forces that account for the interaction between the UAMs. Moreover, in this work we propose a decentralized controller on leader/follower formation that utilizes the derived model of the system. Despite the fact that the UAMs could not have any communication between them, they should estimate the object's direction of movement based only on their onboard sensors. The knowledge of the dynamics of the entire system is necessary when the design of a model-based controller is considered.

The remainder of this article is organized as follows: In Section II, the detailed dynamic model is derived. In Section III, a decentralized control scheme for each UAM is employed, where the leader selects its trajectory and the follower measures the exerted forces and follows the leader. In Section IV, simulation studies are presented, verifying the model and validating the suggested control scheme, followed by concluding remarks.

Throughout the paper, the symbols $c\cdot$ and $s\cdot$ correspond to the cosine and sine of the '$\cdot$'-parameter, respectively. The symbols $\mathbb{I}_{i\times j}$ and $\mathbb{O}_{i\times j}$ stand for the identity and the zero matrix in $\mathbb{R}^{i\times j}$, respectively, while the orthogonal matrix that rotates a vector from A-frame to B-frame is noted as ${}^{B}R_{A} \in \mathbb{R}^{3\times 3}$ satisfying $\left({}^{B}R_{A}\right)^{-1} = \left({}^{B}R_{A}\right)^{\top} = {}^{A}R_{B}$.

II. SYSTEM MODELING

As shown in Fig. 1, we consider two UAVs with their manipulators carrying an object. The interconnection between these two cooperating UAMs is through the object's 6×6 stiffness K_s matrix, characterized by the Young's modulus E, and the associated damping C_s-matrix. It should be noted that no spherical joints are employed at the manipulators' tips to assist in reducing the disturbances of the transmitted forces. In the sequel, we first present the dynamic model of a single UAM, followed by the model that is derived by the interconnection of two UAMs using the stiffness property of the object.

A. SINGLE UAM DYNAMICS

To derive the UAM's dynamic model, the dynamics of the UAV and the dynamic of the n-DoF manipulator should be combined. The Newton-Euler formulation is used to obtain the former dynamics, whilst the RNE approach is employed to extract the later dynamics. The UAV's velocities and accelerations are used in the forward RNE equations of the manipulator followed by the transmitted forces/torques in the base from the reversed RNE equations. In this manner the coupled UAV/manipulator dynamics is computed.

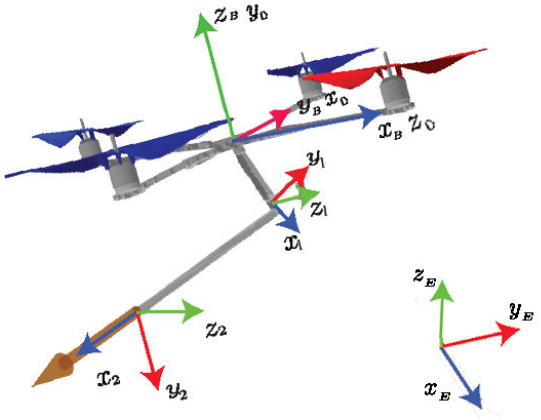

FIGURE 2. Quadrotor with an attached 2 DoF RR-robotic manipulator.

1) UAV-QUADROTOR DYNAMICS

We assume that UAV's CoM coincides with the aerodynamic point of pressure, its propellers are rigid and the thrust and drag forces are proportional to the square of the angular speed of the rotors. In order to describe the UAV's dynamics, we introduce the following coordinate frames: a) the B-frame, or Body-Fixed Frame located on the UAV's CoM, and b) the E-frame, or Earth-Fixed Frame located at the inertial coordinate system origin, as shown in Fig. 2.

The UAV's nonlinear model is derived through the Newton-Euler (N-E) formulation, which describes the combined translational and rotational dynamics of a rigid body. According to this method, the dynamics of a rigid body under the application of external forces and torques, expressed in the B-frame, can be written as

$$\begin{bmatrix} m_s\mathbb{I}_{3\times3} & \mathbb{O}_{3\times3} \\ \mathbb{O}_{3\times3} & I \end{bmatrix}\begin{bmatrix} \dot{v} \\ \dot{\omega} \end{bmatrix} + \begin{bmatrix} \omega \times v \\ \omega \times I\omega \end{bmatrix} = \begin{bmatrix} F \\ \tau \end{bmatrix},$$

where m_s is the total mass and I is the 3×3 moment of inertia about the CoM. The parameters v, ω, correspond to the translational and angular velocity of the CoM, respectively, while F and τ are force and torque vectors acting on the CoM, respectively.

The rotation matrix that allow us to rotate a vector from B-frame to E-frame is

$${}^{E}R_B = \begin{bmatrix} c\theta c\psi & s\phi s\theta c\psi - c\phi s\psi & c\phi s\theta c\psi + s\phi s\psi \\ c\theta s\psi & s\phi s\theta s\psi + c\phi c\psi & c\phi s\theta s\psi - s\phi c\psi \\ -s\theta & s\phi c\theta & c\phi c\theta \end{bmatrix}, \quad (1)$$

where ϕ, θ and ψ are the rotation around x, y and z axes of B-frame, respectively.

Utilizing the N-E method and omitting the friction forces and the disturbances [34], the differential equations describing the UAV's motion are

$$\begin{bmatrix} \dot{V}_E \\ \dot{\omega}_B \end{bmatrix} = \begin{bmatrix} \ddot{x}_c \\ \ddot{y}_c \\ \ddot{z}_c \\ \ddot{\phi} \\ \ddot{\theta} \\ \ddot{\psi} \end{bmatrix} = \begin{bmatrix} u_x \dfrac{U_1}{m_s} \\ u_y \dfrac{U_1}{m_s} \\ -g + (c\phi c\theta)\dfrac{U_1}{m_s} \\ \dot{\theta}\dot{\psi}a_1 + b_1\, U_2 \\ \dot{\phi}\dot{\psi}a_2 + b_2\, U_3 \\ \dot{\theta}\dot{\phi}a_3 + b_3\, U_4 \end{bmatrix}, \quad (2)$$

where $\dot{V}_E = [\ddot{x}_c, \ddot{y}_c, \ddot{z}_c]^\top$ is the translational acceleration of the UAV's CoM expressed in the E-frame, $\dot{\omega}_B = [\ddot{\phi}, \ddot{\theta}, \ddot{\psi}]^\top$ is the angular acceleration expressed in the B-frame and g is the gravitational acceleration. The parameters u_x and u_y indicate the direction of the thrust vector along the x and y axes in the E-frame and are defined as:

$$u_x = c\phi s\theta c\psi + s\phi s\psi, \quad u_y = c\phi s\theta s\psi - s\phi c\psi. \quad (3)$$

The parameters $a_i, b_i,\ i = 1, 2, 3$, are:

$$\begin{aligned} a_1 &= \frac{I_{yy} - I_{zz}}{I_{xx}}, \quad b_1 = \frac{l_a}{I_{xx}}, \\ a_2 &= \frac{I_{zz} - I_{xx}}{I_{yy}}, \quad b_2 = \frac{l_a}{I_{yy}}, \\ a_3 &= \frac{I_{xx} - I_{yy}}{I_{zz}}, \quad b_3 = \frac{1}{I_{zz}}, \end{aligned} \quad (4)$$

where l_a is the arm length of the UAV, I_{xx}, I_{yy} and I_{zz} is the moment of inertia of the UAV about the x, y and z axes, respectively.

The control inputs $U_1, U_2, U_3, U_4 \in \mathbb{R}$ are defined to make our model independent of the shape and the number of the UAV's rotors. The input U_1 is the total thrust in B_z axis, while the inputs U_2, U_3 and U_4 are related to the torques on the UAV around B_x,B_y and B_z axes, respectively.

2) ROBOTIC MANIPULATOR DYNAMICS

Let the Base-Fixed Frame (O-frame) be located at the base of the manipulator; while the UAV is moving, the position and the orientation of the O-frame change over time following that of the UAV. Rather than using the Euler-Lagrange equations in [35] or the Gibbs-Appell formulation in [36] to derive the dynamics of a robotic manipulator, the N-E equations [37] will be employed. This recursive force-based method is typically used for floating-base manipulators, where the velocities and accelerations of the base link correspond to a nonzero value. These velocities and accelerations are in turn transmitted from one link to another by a forward recursion and would result in additional resultant forces and torques computed by a backward recursion. Most manipulators are not using translational joints, therefore we will present the RNE for manipulators with rotational, only, type of joints, instead of a generic manipulator.

Forward Recursion: In this first stage, the linear and angular velocities and accelerations of each link are calculated recursively in terms of its preceding link, starting from the

base to the end-effector. The initial conditions for the base link are v_0, $\dot{v}_0$ and ω_0, $\dot{\omega}_0$. With this initialization the forward Recursion equations are calculated for $i = 1, \ldots, n$ as

$$
\begin{aligned}
{}^{i}R_0\omega_i &= {}^{i}R_{i-1}\left({}^{i-1}R_0\omega_{i-1} + z_0\dot{q}_i\right),\\
{}^{i}R_0\dot{\omega}_i &= {}^{i}R_{i-1}\left({}^{i-1}R_0\dot{\omega}_{i-1} + z_0\ddot{q}_i + \left({}^{i-1}R_0\omega_{i-1}\right)\times z_0\dot{q}_i\right),\\
{}^{i}R_0\dot{v}_i &= \left({}^{i}R_0\dot{\omega}_i\right)\times\left({}^{i}R_0p_i^*\right) + {}^{i}R_{i-1}\\
&\quad + \left({}^{i}R_0\omega_i\right)\times\left(\left({}^{i}R_0\omega_i\right)\times\left({}^{i}R_0p_i^*\right)\right)\left({}^{i-1}R_0\dot{v}_{i-1}\right),\\
{}^{i}R_0\bar{a}_i &= \left({}^{i}R_0\dot{\omega}_i\right)\times\left({}^{i}R_0\bar{s}_i\right) + {}^{i}R_0\dot{v}_i\\
&\quad + \left({}^{i}R_0\omega_i\right)\times\left(\left({}^{i}R_0\omega_i\right)\times\left({}^{i}R_0\bar{s}_i\right)\right),
\end{aligned}
$$

where $\bar{s}_i$ is the position of the CoM i from the origin of the i-th local coordinate system and p_i^* is the origin of the i-th coordinate frame with respect to the $(i-1)$-th coordinate system. The parameters ω_i and v_i are the angular and linear velocity of the CoM of link i, respectively. The linear acceleration of the CoM of link i is the $\bar{a}_i$ and the parameter q_i denotes the rotational parameter (angle) of link i. Finally, $z_0 = [0,\ 0,\ 1]^\top$.

Backward Recursion: Having computed the velocities and accelerations of all links, the second stage of the RNE starts by computing the joint forces/torques for each link starting from the end-effector towards the base. The required backward Recursion equations are calculated for $i = n, \ldots, 1$ as

$$
{}^{i}R_0f_i = {}^{i}R_{i+1}\left({}^{i+1}R_0f_{i+1}\right) + m_i{}^{i}R_0\bar{a}_i, \tag{5}
$$

$$
\begin{aligned}
{}^{i}R_0\eta_i &= {}^{i}R_{i+1}\left({}^{i+1}R_0\eta_{i+1} + \left({}^{i+1}R_0p_i^*\right)\times\left({}^{i+1}R_0f_{i+1}\right)\right)\\
&\quad + \left({}^{i}R_0p_i^* + {}^{i}R_0\bar{s}_i\right)\times\left({}^{i}R_0F_i\right)\\
&\quad + \left({}^{i}R_0I_i{}^{0}R_i\right)\left({}^{i}R_0\dot{\omega}_i\right)\\
&\quad + \left({}^{i}R_0\omega_i\right)\times\left(\left({}^{i}R_0I_i{}^{0}R_i\right)\left({}^{i}R_0\omega_i\right)\right),
\end{aligned} \tag{6}
$$

$$
\tau_i = \left({}^{i}R_0\eta_i\right)^\top\left({}^{i}R_{i-1}z_0\right), \tag{7}
$$

where m_i is the mass of link i, $F_i = m_i\bar{a}_i$ is the total external force exerted on link i at its CoM, I_i is the inertia matrix of link i about its CoM with reference to the (i)-th frame, f_i is the force exerted on link i by link $i-1$ at the $(i-1)$-th local coordinate frame to support link i and the following links to it and η_i is the moment exerted on link i by link $i-1$ at the $(i-1)$-th local coordinate frame. The initial conditions for the backward recursion are defined by the load affecting the end-effector of the robotic manipulator. Aggregating (7) in a symbolic manner leads to the classical model

$$
D^R(q)\ddot{q} + C^R(q,\dot{q})\dot{q} + G^R(q) = \tau^R, \tag{8}
$$

where $q \in \mathbb{R}^n$ is the vector of joint variables, $D^R(q) \in \mathbb{R}^{n\times n}$ is the generalized inertia matrix, $C^R(q) \in \mathbb{R}^n$ is the Coriolis matrix, $G^R(q) = [g_1(q), \ldots, g_n(q)]^\top$ is the gravity vector and $\tau^R = [\tau_1, \tau_2, \ldots, \tau_n]^\top$ is the vector of torques.

3) MODELING OF THE COUPLED UAV/MANIPULATOR SYSTEM

Assuming that the manipulator is placed on the UAV's CoM the initial conditions are:

$$
\begin{aligned}
v_0 &= {}^{O}R_EV_E,\ \dot{v}_0 = {}^{O}R_E\left(\dot{V}_E + [0\quad 0\quad g]^\top\right),\\
\omega_0 &= {}^{O}R_B\omega_B,\ \dot{\omega}_0 = {}^{O}R_B\dot{\omega}_B,
\end{aligned} \tag{9}
$$

where v_0, $\dot{v}_0$, $(\omega_0,\ \dot{\omega}_0)$ are the translational (angular) velocities and accelerations of the UAV with respect to the O-frame, while the matrices ${}^{O}R_E$ and ${}^{O}R_B$ are

$$
{}^{O}R_B = \begin{bmatrix} 0 & 1 & 0\\ 0 & 0 & 1\\ 1 & 0 & 0\end{bmatrix},\quad {}^{O}R_E = {}^{O}R_B{}^{B}R_E. \tag{10}
$$

The RNE allow the computation of the force and torque applied on the center of mass of the UAV due to the interconnection with the manipulator in terms of (5)-(6). Hence, the reaction forces and torques to the manipulator's base with respect to the O-frame can be obtained as

$$
f_0 = {}^{0}R_1f_1,\quad \eta_0 = {}^{0}R_1\eta_1. \tag{11}
$$

Expressing the force (torque) vector in the E (B)-frame yields

$$
f_E = \left({}^{O}R_E\right)^{-1}f_0,\quad \eta_B = \left({}^{O}R_B\right)^{-1}\eta_0, \tag{12}
$$

where

$$
\begin{aligned}
f_E &= \left[f_{E,x},\ f_{E,y},\ f_{E,z}\right]^\top\\
\eta_B &= \left[\eta_{B,x},\ \eta_{B,y},\ \eta_{B,z}\right]^\top.
\end{aligned}
$$

These reaction forces/torques affect the dynamic equations (2) as

$$
\begin{bmatrix}\dot{V}_E^r\\ \dot{\omega}_B^r\end{bmatrix} = \begin{bmatrix}\dot{V}_E\\ \dot{\omega}_B\end{bmatrix} - \begin{bmatrix}f_E\\ \eta_B\end{bmatrix}. \tag{13}
$$

The computation of the RNE provides us with the forces and torques that are applied to the UAV due to the interconnection with the manipulator. Thus, combining (7) which describes the dynamic model of the floating manipulator, with (13) that describes a UAV subject to the forces from the interconnected manipulator, can yield the model of the coupled system. Rather than relying on the recursive nature of the dynamic equations, the derived equations can be combined using a symbolic manipulation package [38], yielding a system with a $6+n$ vector and its derivative (total of $2\times(6+n)$ states). Let $x = [x_c, y_c, z_c, \phi, \theta, \psi, q_1, \ldots, q_n]^\top$; then the dynamic equations can be written as

$$
D(x)\ddot{x} + G(x) + C(x,\dot{x})\dot{x} = \tau_c + J^\top(x)F_e, \tag{14}
$$

where $D(x)$ is UAM's symmetric inertial matrix, $G(x)$ the gravitational vector, the Coriolis vector $C(x,\dot{x})\dot{x}$, τ_c the $(6+n)$ input vector, F_e the external applied forces and $J(x)$ the Jacobian matrix of the system.

The structure of the matrix $D_{(6+n)\times(6+n)}(x)$ is

$$
D(x) = \left[\begin{array}{c|c} D^Q_{6\times6}(q) & D^{RQ}_{6\times n}(x)\\ \hline \left[D^{RQ}(x)\right]^\top & D^R_{n\times n}(q)\end{array}\right]. \tag{15}
$$

In matrix $D(x)$, the submatrix D^Q depends, not only, on the mass and the moment of inertia of the UAV, but also on the configuration of the attached manipulator. The submatrix D^R is the inertial matrix of a fixed based manipulator, whereas the submatrix D^{RQ} expresses the interaction between the manipulator and the UAV.

Assuming that the gravity vector is along the negative z-axis, we can write $G = g\,[\mathbb{O}_{1\times 6}, G_7, \ldots, G_{6+n}]^\top$, where $G_i(x)$ with $i \in \{3, 4, \ldots, 6+n\}$ depends on the configuration of both the UAV and the manipulator. The matrix $C_{(6+n)\times(6+n)}$ encapsulates the Coriolis and centrifugal generalized forces and it accommodates the terms related with the linear and the angular velocities of the system.

Finally, we have the $\tau_c = Bu$, where the $(6+n)\times(4+n)$ actuator assignment matrix B is

$$B(\phi,\theta,\psi) = \left[\begin{array}{cccc|c} c\varphi\, c\psi\, s\vartheta + s\varphi\, s\psi & 0 & 0 & 0 & \\ c\varphi\, s\psi\, s\vartheta - s\varphi\, c\psi & 0 & 0 & 0 & \\ c\varphi\, c\vartheta & 0 & 0 & 0 & \mathbb{O}_{6\times n} \\ 0 & l_a & 0 & 0 & \\ 0 & 0 & l_a & 0 & \\ 0 & 0 & 0 & 1 & \\ \hline \multicolumn{4}{c|}{\mathbb{O}_{n\times 4}} & \mathbb{I}_{n\times n} \end{array}\right],$$

while the vector u, containing the systems inputs, consists of: a) the four UAV-aerodynamic induced parameters U_1, U_2, U_3, U_4, and b) the n-torques, applied to the manipulator's joints. Therefore,

$$\begin{aligned} u &= \left[U_1, U_2, U_3, U_4, \tau^R\right]^\top \\ &= [U_1, U_2, U_3, U_4, \tau_1, \tau_2, \ldots, \tau_n]^\top. \end{aligned}$$

The UAM interacts with the environment through the term $F_e = [F_x,\ F_y,\ F_z,\ \tau_x,\ \tau_y,\ \tau_z]^\top$, where F_x, F_y, F_z (τ_x, τ_y, τ_z) are the applied forces (torques) along (around) the x, y and z axes of the last coordinate system of the robot manipulator. The Jacobian matrix J can be decomposed as

$$J = \left[J^Q(x)_{6\times 6} \middle| \left[\begin{array}{c|c} {}^B R_n & \mathbb{O}_{3\times 3} \\ \hline \mathbb{O}_{3\times 3} & {}^B R_n \end{array}\right] J^R(q)_{6\times n} \right]_{6\times(6+n)}, \quad (16)$$

where the matrix $J^Q(x)$ describes the interaction of the applied forces at the robot's end-effector to the UAV's base, while $J^R(q)$ is the Jacobian matrix of a fixed based manipulator under the assumption that the UAV hovers.

B. LEADER/FOLLOWER UAM DYNAMICS

In a leader/follower UAM formation, as shown in Fig. 3, concatenation of the individual member equations yields the overall model, while the carried object is acting as a coupling between this pair of UAMs.

The leader/follower system dynamic model is an extension from (14) resulting in a state vector composed of the states of the leader and follower UAMs. Hence, the state of the combined system is $x = \left[x^l, x^f\right]^\top$, where the superscript $^{l(f)}$ refers to the leader (follower) and $x^l = \left[x_c^l, y_c^l, z_c^l, \phi^l, \theta^l, \psi^l, q_1^l, \ldots, q_n^l\right]^\top$, followed by a similar notation for x^f. The resulting system dynamics is

$$\begin{aligned} &\left[\begin{array}{c|c} D^l(x^l) & \overline{\mathbb{O}} \\ \hline \overline{\mathbb{O}} & D^f(x^f) \end{array}\right]\left[\begin{array}{c} \ddot{x}^l \\ \hline \ddot{x}^f \end{array}\right] + \left[\begin{array}{c} G^l(x^l) \\ \hline G^f(x^f) \end{array}\right] \\ &\quad + \left[\begin{array}{c|c} C^l(x^l,\dot{x}^l) & \overline{\mathbb{O}} \\ \hline \overline{\mathbb{O}} & C^f(x^f,\dot{x}^f) \end{array}\right]\left[\begin{array}{c} \dot{x}^l \\ \hline \dot{x}^f \end{array}\right] \\ &\quad = \left[\begin{array}{c} \tau_c^l \\ \hline \tau_c^f \end{array}\right] + \left[\begin{array}{c|c} J^l(x^l)^\top & \overline{\mathbb{O}^r} \\ \hline \overline{\mathbb{O}^r} & J^f(x^f)^\top \end{array}\right]\left[\begin{array}{c} F^l \\ \hline F^f \end{array}\right], \end{aligned} \quad (17)$$

where $\overline{\mathbb{O}} = \mathbb{O}_{(6+n)\times(6+n)}$ and $\overline{\mathbb{O}^r} = \mathbb{O}_{6\times(6+n)}$.

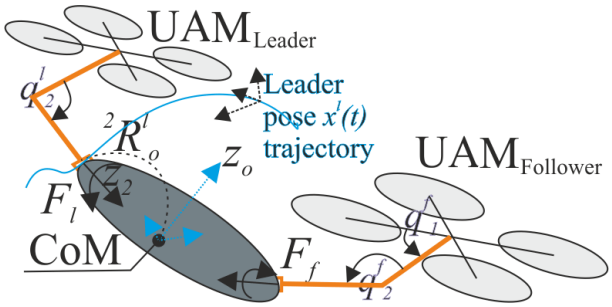

FIGURE 3. Leader/Follower UAM formation.

The leader UAM applies a force to the object that can cause small translation and rotation around its center of mass. The follower UAM attempts to follow the leader UAM resulting in a reaction force applied to it. Under the assumption of a grabbed object by both robots' grippers, the exercised forces F^l and F^f are related to the object's stiffness.

Let a coordinate system be assigned at the object's center of mass with its orientation aligned along the principal axes of the object. The rotational transformation that aligns the axes of the leader's end effector coordinate system to the assigned one is ${}^nR_o^l$. Assume the object has a homogeneous mass density and let its stiffness matrix be K_o and a diagonal damping matrix $C_o = \mathrm{diag}(c_x^l, c_y^l, c_z^l, ..)^\top$. The applied force by the follower is

$$F^l = \left[\begin{array}{c} \overline{F}^l \\ \hline \overline{\tau}^l \end{array}\right] = \left[\begin{array}{c|c} {}^nR_o^l & \mathbb{O}_{3\times 3} \\ \hline \mathbb{O}_{3\times 3} & {}^nR_o^l \end{array}\right]\left\{K_o\left[\begin{array}{c} \overline{x}^l \\ \hline \overline{r}^l \end{array}\right] + C_o\left[\begin{array}{c} \dot{\overline{x}}^l \\ \hline \dot{\overline{r}}^l \end{array}\right]\right\},$$

where the vector $\left[\overline{x}^l|\overline{r}\right]^\top = \left[dx^l, dy^l, dz^l|d\phi^l, d\theta^l, d\psi^l\right]^\top$ corresponds to the differential translation and rotation of the carried object under tension/compression and torsion.

Similarly, the generalized force applied at the follower end effector is

$$F^f = \left[\begin{array}{c} \overline{F}^f \\ \hline \overline{\tau}^f \end{array}\right] = \left[\begin{array}{c|c} {}^nR_o^f & \mathbb{O}_{3\times 3} \\ \hline \mathbb{O}_{3\times 3} & {}^nR_o^f \end{array}\right]\left\{K_o\left[\begin{array}{c} \overline{x}^f \\ \hline \overline{r}^f \end{array}\right] + C_o\left[\begin{array}{c} \dot{\overline{x}}^f \\ \hline \dot{\overline{r}}^f \end{array}\right]\right\}.$$

Essentially, the carried objects act as the coupler in the leader/follower formation.

III. SYSTEM CONTROL

A decentralized control scheme was employed relying on the leader-follower formation, as shown in Fig. 4. The leader moves along a predefined trajectory, while the follower is

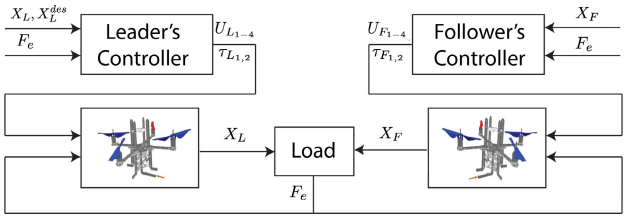

FIGURE 4. Control strategy for the entire system.

attempting to maintain a desired pose with respect to the leader [39]. Hence, the leader UAM is responsible for the load transportation trajectory, while the follower is trying to reduce the internal forces of the system by complying with the trajectory planned by the leader. The only information indirectly passed between the leader and follower is through the exercised forces via the carried object.

A. LEADER CONTROLLER DESIGN

Model-dependent controllers [40] are capable of maintaining the pose of the UAM despite the force exerted by the manipulator. The carried manipulator is controlled using a feedback linearization scheme to track the reference trajectory, while a modified Proportional-Derivative (PD) controller accounting for the total mass m_t^l of the leader UAM and its applied forces is employed for the leader UAV.

1) LEADER UAV CONTROLLER

The leader UAV generates the necessary thrust to eliminate the external generalized forces acting on it, otherwise the leader UAV will either push or pull the follower UAV. Given the following quantities for the leader UAV: a) the desired altitude z_d^l, the desired orientation angles $\phi_d^l(\theta_d^l)[\psi_d^l]$ roll(pitch)[yaw] and the desired angular velocities $\dot{\phi}_d^l(\dot{\theta}_d^l)[\dot{\psi}_d^l]$, b) the inertial moment of the UAV I_{xx}^l, I_{yy}^l and I_{zz}^l, c) the mass m_t^l of the UAM, and d) the measured altitude z^l, orientation angles ϕ^l, θ^l and ψ^l and angular velocities $\dot{\phi}^l, \dot{\theta}^l$ and $\dot{\psi}^l$, the controller initially computes

$$U_1^l = \frac{m_t^l}{c\phi^l c\theta^l}\left(g - k_{z,d}^l\left(\dot{z}^l - \dot{z}_d^l\right) - k_{z,p}^l\left(z^l - z_d^l\right)\right),$$

$$U_2^l = \frac{I_{xx}^l}{l_a^l}\left(-\dot{\theta}^l\dot{\psi}^l\alpha_1^l - k_{\phi,d}^l\left(\dot{\phi}^l - \dot{\phi}_d^l\right) - k_{\phi,p}^l\left(\phi^l - \phi_d^l\right)\right),$$

$$U_3^l = \frac{I_{yy}^l}{l_a^l}\left(-\dot{\phi}^l\dot{\psi}^l\alpha_2^l - k_{\theta,d}^l\left(\dot{\theta}^l - \dot{\theta}_d^l\right) - k_{\theta,p}^l\left(\theta^l - \theta_d^l\right)\right),$$

$$U_4^l = I_{zz}^l\left(-\dot{\phi}^l\dot{\theta}^l\alpha_3^l - k_{\psi,d}^l\left(\dot{\psi}^l - \dot{\psi}_d^l\right) - k_{\psi,p}^l\left(\psi^l - \psi_d^l\right)\right).$$

The aforementioned equations concern a feedback linearization controller for a UAV without manipulator, where it should be noted that we used the superscript l to denote the leader UAV parameters. Therefore, to account for the reaction forces from the manipulator to the UAV (13), the equations must be modified as:

$$\begin{aligned} U_1^l &= U_1^l, \\ U_2^l &= U_2^l + \frac{I_{xx}^l}{l_a^l}\,\eta_{B,x}^l, \\ U_3^l &= U_3^l + \frac{I_{yy}^l}{l_a^l}\,\eta_{B,y}^l, \\ U_4^l &= U_4^l + I_{zz}^l\,\eta_{B,z}^l. \end{aligned} \tag{18}$$

It can be shown that the resulting closed loop system is stable. Hence, we define the Lyapunov candidate function, which is positive defined, if $k_{\phi,p}^l, k_{\theta,p}^l, k_{\psi,p}^l > 0$.

$$V = \frac{1}{2}(k_{\phi,p}^l e_\phi^2 + k_{\theta,p}^l e_\theta^2 + k_{\psi,p}^l e_\psi^2) + \frac{1}{2}(\dot{e}_\phi^2 + \dot{e}_\theta^2 + \dot{e}_\psi^2),$$

where

$$\begin{aligned} e_\phi &= \phi_d^l - \phi^l,\ \dot{e}_\phi = \dot{\phi}_d^l - \dot{\phi}^l,\ \ddot{e}_\phi = \ddot{\phi}_d^l - \ddot{\phi}^l, \\ e_\theta &= \theta_d^l - \theta^l,\ \dot{e}_\theta = \dot{\theta}_d^l - \dot{\theta}^l,\ \ddot{e}_\theta = \ddot{\theta}_d^l - \ddot{\theta}^l, \\ e_\psi &= \psi_d^l - \psi^l,\ \dot{e}_\psi = \dot{\psi}_d^l - \dot{\psi}^l,\ \ddot{e}_\psi = \ddot{\psi}_d^l - \ddot{\psi}^l. \end{aligned}$$

The first derivative of the Lyapunov function V is:

$$\begin{aligned} \dot{V} &= k_{\phi,p}^l e_\phi \dot{e}_\phi + k_{\theta,p}^l e_\theta \dot{e}_\theta + k_{\psi,p}^l e_\psi \dot{e}_\psi \\ &\quad + \dot{e}_\phi \ddot{e}_\phi + \dot{e}_\theta \ddot{e}_\theta + \dot{e}_\psi \ddot{e}_\psi \\ \dot{V} &= -k_{\phi,d}^l(\dot{e}_\phi)^2 - k_{\theta,d}^l(\dot{e}_\theta)^2 - k_{\psi,d}^l(\dot{e}_\psi)^2, \end{aligned}$$

which is negative defined, if $k_{\phi,d}^l, k_{\theta,d}^l, k_{\psi,d}^l > 0$. Thus, the system is stable in the sense of Lyapunov.

2) LEADER MANIPULATOR CONTROLLER

A classical feedback linearization scheme, relying on computed torque controller is employed for the manipulator

$$\begin{aligned} \tau_c^l = {} & D^{R,l}(x^l)\left[-\ddot{q}_d^l + K_d^l\left(\dot{q}^l - \dot{q}_d^l\right) + K_p^l\left(q^l - q_d^l\right)\right] \\ & - \left({}^B R_n^l J^{R,l}(q^l)\right)^\top F^l + g\left[G_7^l(x^l), \ldots, G_{6+n}^l(x^l)\right]^\top \\ & + \left[\mathbb{O}_{n\times 6}\middle|\mathbb{I}_{n\times n}\right] C^l\left(x^l, \dot{x}^l\right)\dot{x}^l, \end{aligned} \tag{19}$$

where q_d^l corresponds to the desired angle vector of the attached manipulator and K_p, K_d positively defined matrices. It should be noted that when the leader-UAV hovers ($\phi^l = \theta^l = \psi^l = 0$) and has a large mass(inertia) compared to its attached manipulator, then (19) degenerates to

$$\begin{aligned} \tilde{\tau}_c^l = {} & \tilde{D}^{R,l}(q^l)\left[-\ddot{q}_d^l + K_d^l\left(\dot{q}^l - \dot{q}_d^l\right) + K_p^l\left(q^l - q_d^l\right)\right] \\ & - \left({}^B R_n^l \tilde{J}^{R,l}(q^l)\right)^\top F^l + g\left[\tilde{G}_7^l(q^l), \ldots, \tilde{G}_{6+n}^l(q^l)\right]^\top \\ & + \left[\mathbb{O}_{n\times 6}\middle|\mathbb{I}_{n\times n}\right] \tilde{C}^l\left(q^l, \dot{q}^l\right)\dot{q}^l, \end{aligned} \tag{20}$$

where the $\tilde{\cdot}$ quantities correspond to those of a rigidly attached manipulator. The $q_d^l, \dot{q}_d^l, \ddot{q}_d^l$ desired trajectories are selected according to the specifications.

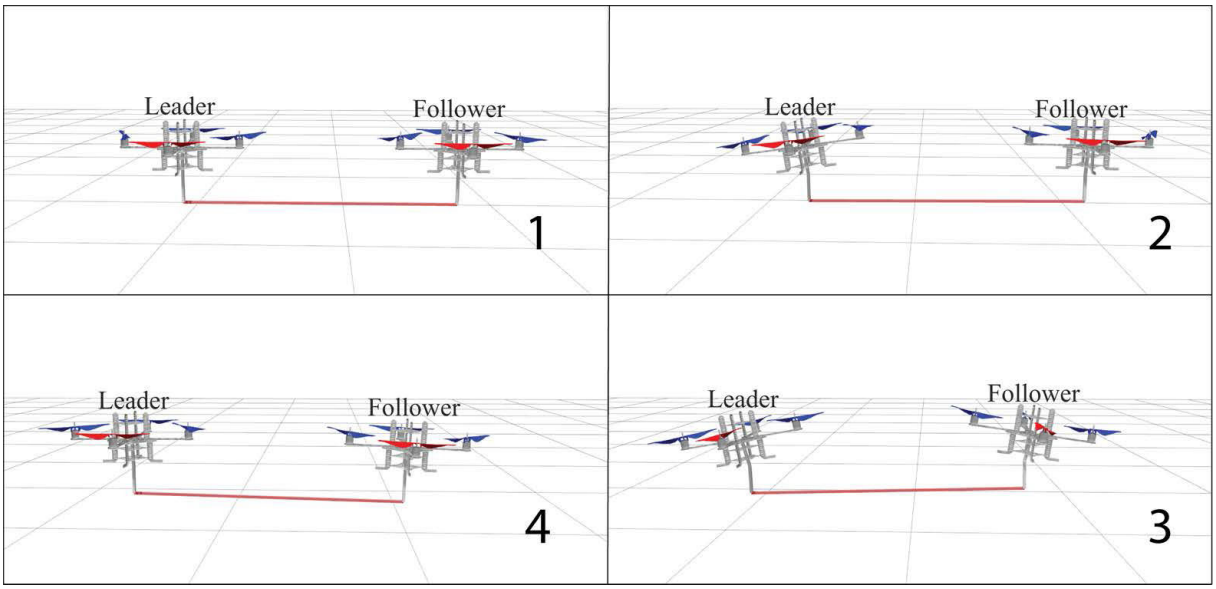

FIGURE 5. Leader/Follower Controller Gazebo-snapshots.

B. FOLLOWER UAM CONTROLLER

1) FOLLOWER UAV CONTROLLER

Rather than communicating with the leader-UAV for receiving information about its state vector x^l and F^l, the follower-UAV's control relies solely on the measured force F^f. In a static configuration, where both leader and follower hover while carrying the object, $F^l + F^f = [0, 0, m_l g, 0, 0, 0]^\top$, where m_l is the object's mass since both contribute to carry the object.

If the leader moves, then the elements of this vector will change and the follower's controller will attempt to reduce this variation by moving in a direction that compensates against this change. In the general case, the follower computes the following desired altitude and attitude velocities

$$\begin{bmatrix} \dot{x}_d^f \\ \dot{y}_d^f \\ \dot{z}_d^f \\ \dot{\phi}_d^f \\ \dot{\theta}_d^f \\ \dot{\psi}_d^f \end{bmatrix} = \beta \left(F^f - \begin{bmatrix} 0 \\ 0 \\ m_o g \\ 0 \\ 0 \\ 0 \end{bmatrix} \right), \tag{21}$$

where $\beta \geq 0$ is a parameter affecting the speed of the system's transient response. To generate the proper attitude inputs for the UAM, we used the geometric tracking control in [41] for the desired trajectory defined in (21).

The inputs for the controller of the follower UAV can be written as

$$U_1^f = \frac{m_s^f + \sum_{i=1}^n m_i^f}{c\phi^f c\theta^f} \left(g - k_{z,d}^f \left(\dot{z}^f - \dot{z}_d^f \right) - k_{z,p}^f \left(z^f - z_d^f \right) \right),$$
$$U_2^f = \frac{I_{xx}^f}{l_a^f} \left(-\dot{\theta}^f \dot{\psi}^f \alpha_1^f - k_{\phi,d}^f \left(\dot{\phi}^f - \dot{\phi}_d^f \right) - k_{\phi,p}^f \left(\phi^f - \phi_d^f \right) \right),$$
$$U_3^f = \frac{I_{yy}^f}{l_a^f} \left(-\dot{\phi}^f \dot{\psi}^f \alpha_2^f - k_{\theta,d}^f \left(\dot{\theta}^f - \dot{\theta}_d^f \right) - k_{\theta,p}^f \left(\theta^f - \theta_d^f \right) \right),$$
$$U_4^f = I_{zz}^f \left(-\dot{\phi}^f \dot{\theta}^f \alpha_3^f - k_{\psi,d}^f \left(\dot{\psi}^f - \dot{\psi}_d^f \right) - k_{\psi,p}^f \left(\psi^f - \psi_d^f \right) \right). \tag{22}$$

This algorithm can easily navigate the follower UAV in an obstacle free environment, otherwise due to the interconnecting object the path planning algorithm needs to be modified to account for the finite size of the leader/follower.

2) FOLLOWER MANIPULATOR CONTROLLER

The controller for the manipulator of the follower UAM is identical in structure to the controller of the manipulator of the leader UAM, excluding the term referring to the elimination of the forces on its gripper.

$$\begin{aligned} \tilde{\tau}_c^f = {} & \tilde{D}^{R,f}(q^f) \left[-\ddot{q}_d^f + K_d^f \left(\dot{q}^f - \dot{q}_d^f \right) + K_p^f \left(q^f - q_d^f \right) \right] \\ & + g \left[\tilde{G}_7^f(q^f), \ldots, \tilde{G}_{6+n}^f(q^f) \right]^\top \\ & + \left[\mathbb{O}_{n\times 6} | \mathbb{I}_{n\times n} \right] \tilde{C}^f \left(q^f, \dot{q}^f \right) \dot{q}^f, \end{aligned} \tag{23}$$

where the parameters q_d^f, $\dot{q}_d^f$, $\ddot{q}_d^f$ are the desired trajectories.

The UAM-leader's controllers are defined in (18) and (19), while the ones for the follower appear in (21), (22) and (23).

IV. SIMULATION STUDIES

In the following simulations, we study the leader/follower UAM-formation illustrated in Fig. 6. Each quadrotor UAM has a two DoF rotational manipulator ($n = 2$) attached to its center and both UAMs carry an object almost parallel to the ground. The leader's first link reference angle is perpendicular ($q_{d,1}^l = 90°$) to its aerodynamic plane, while its second link reference angle is adjusted so that it points perpendicular

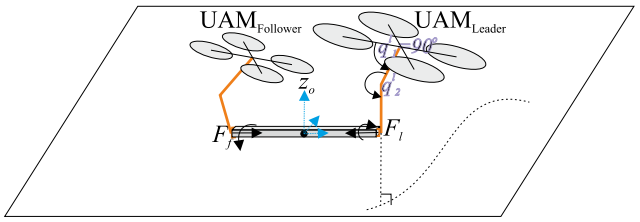

FIGURE 6. Leader/Follower UAM formation carrying a beam.

to the ground. The follower's manipulator reference angles follow the same guidelines as those of the leader's manipulator, with the objective to keep the object (beam) parallel to the ground.

The propellers' rotational speeds $\Omega_i,\ i = 1,\ldots,4$ are mapped to the inputs $U_i,\ i = 1,\ldots,4$, using

$$\begin{bmatrix} U_1 \\ U_2 \\ U_3 \\ U_4 \end{bmatrix} = \begin{bmatrix} b & b & b & b \\ 0 & -b & 0 & b \\ b & 0 & -b & 0 \\ -d & d & -d & d \end{bmatrix} \begin{bmatrix} \Omega_1^2 \\ \Omega_2^2 \\ \Omega_3^2 \\ \Omega_4^2 \end{bmatrix}, \tag{24}$$

where the parameters b and d correspond to the UAV's thrust and drag coefficient, respectively.

These UAMs carry a simple beam with the following stiffness and damping matrices

$$K_o = \frac{E}{L^2} \begin{bmatrix} \frac{12I}{L} & 0 & 0 & 0 & 0 & 6I \\ 0 & AL & 0 & 0 & 0 & 0 \\ 0 & 0 & \frac{12I}{L} & 6I & 0 & 0 \\ 0 & 0 & 6I & 4I & 0 & 0 \\ 0 & 0 & 0 & 0 & 4I & 0 \\ 6I & 0 & 0 & 0 & 0 & 4I \end{bmatrix}$$

$$C_o = \text{diag}\left(c_x^l, c_y^l, c_z^l, c_x^r, c_y^r, c_z^r\right),$$

where E is the Young's modulus of elasticity, L is the length of the beam, A is the area of the cross-section perpendicular to the applied force and I is the beam's area moment of inertia. The parameter $c_i^l(c_i^r),\ i = x, y, z$ is the load's linear (rotational) damping along the i-axis.

The main platform for the simulation studies relies on the "RotorS" simulator [42], which is a micro air vehicle Gazebo physics engine simulator, that has embedded several multirotor UAVs. Each used UAM consists of a "Pelican" quadrotor [43] and a two-link serial manipulator, as shown in Fig. 2. Comparisons between the Gazebo engine and the dynamic equations implemented in Matlab were also investigated. The UAM parameters for the simulation are provided in Table 1.

Snapshots of the simulation are shown in Fig. 5. In snapshot #1, the system is in equilibrium waiting for the destination position. In snapshot #2, the leader UAM moves and attempts to pull the follower UAM. The follower UAM moves in snapshot #3 and attempts to self-stabilize itself. In the 4th snapshot, the leader UAM has arrived at its destination and provides an indirect command, through the forces applied to the object, to the follower UAM to stop its motion.

TABLE 1. UAM parameters.

UAV moment of inertia	I_{xx}	0.01	$[kg \cdot m^2]$
UAV moment of inertia	I_{yy}	0.01	$[kg \cdot m^2]$
UAV moment of inertia	I_{zz}	0.02	$[kg \cdot m^2]$
UAV mass	m_s	1	$[kg]$
UAV arm length	l_a	0.21	$[m]$
UAV thrust coefficient	b	8e-5	$[N \cdot s^2]$
UAV drag coefficient	d	1e-6	$[N \cdot m \cdot s^2]$
1st Link mass	m_1	0.1	$[kg]$
1st Link length	l_1	0.1	$[m]$
1st Link inertia	I_1	0.02	$[kg \cdot m^2]$
2nd Link mass	m_2	0.1	$[kg]$
2nd Link length	l_2	0.1	$[m]$
2nd Link inertia	I_2	0.02	$[kg \cdot m^2]$
Load's Young's modulus	E	1e10	$[N/m^2]$
Load's mass	m_l	0.8	$[kg]$
Load damping	c_l	2e-1	$[N \cdot s/m]$
Rotational damping	c_r	2e-1	$[N \cdot m \cdot s/rad]$

A. SIMULATION STUDY I

The overall leader/follower UAM system has 32 states and partial results from the study appear in Fig. 7. The reference movement consists of translation on all axes and changes in both angles of the manipulator for both UAMs. The UAV was asked to move from its hovering state with a 1 m step command (at $t = 0$) applied along the y-axis, followed by 1 m step along the x (at $t = 5$ s) and, finally, a 1 m step backwards in y-axis (at $t = 10$ s).

The attached manipulators point perpendicular to the ground for both leader and follower while their first joint angle is perpendicular to its aerodynamic plane of pressure. Each system uses the same PD-parameters in (19) and (23) and attempts to carry the beam-object almost parallel to the ground. The parameters for the PD of the manipulator are $K_p^f = K_p^l = \text{diag}(0.1, 0.01)$ and $K_d^f = K_d^l = \text{diag}(0.01, 0.001)$, while the parameters for the UAV can be found in [42].

In the simulation comparison, between the Gazebo physics engine and Matlab, shown in Fig. 7, it can be seen that the deviation is negligible, with a maximum error of $0.04m$ indicating a close match. Hence, having used the same inputs with the same parameters in both simulations, we consider that the model presented in this work is a valid description of the system's dynamics. Similarly, the applied forces/torques from the leader appear in Fig. 10, for the simulation case, shown in Fig. 7. As anticipated, at $t = 5$ and $t = 10$ seconds due to

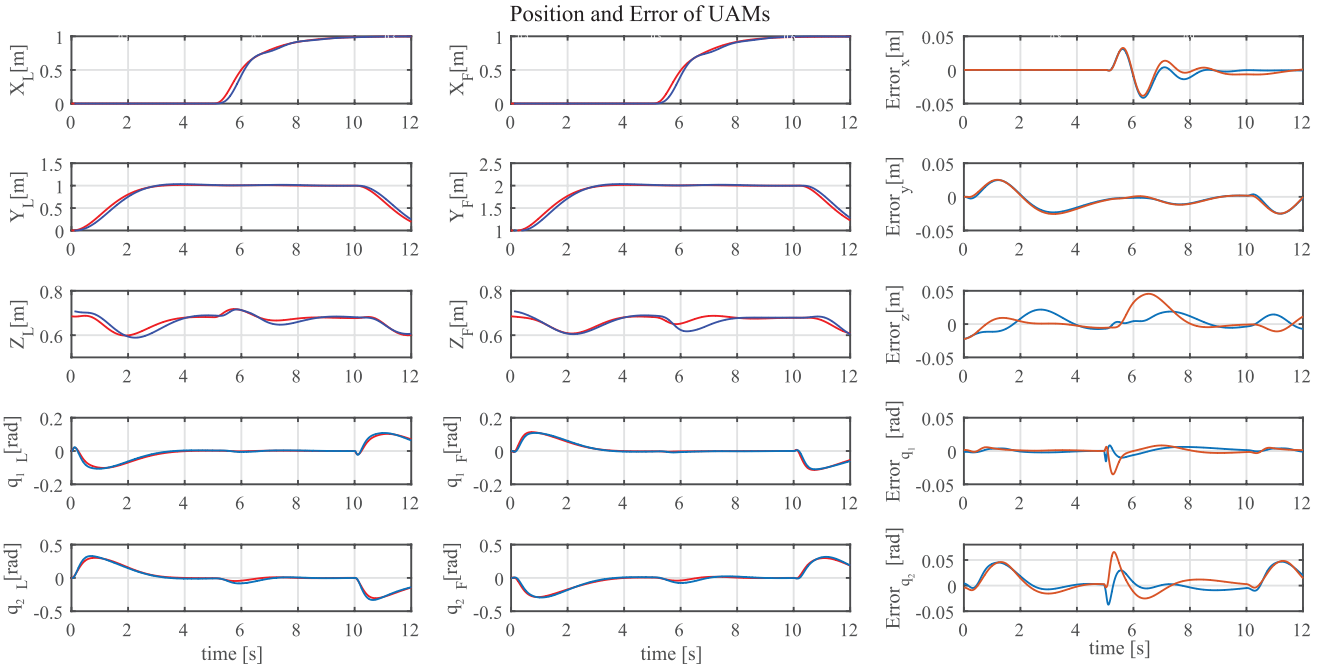

FIGURE 7. Model comparison between Gazebo (red) and Matlab (blue) simulators. The first (second) column refers to the leader (follower) UAV. The relative error between the simulator engines is shown in the third column. The leader (follower) UAM error is shown in cyan (orange).

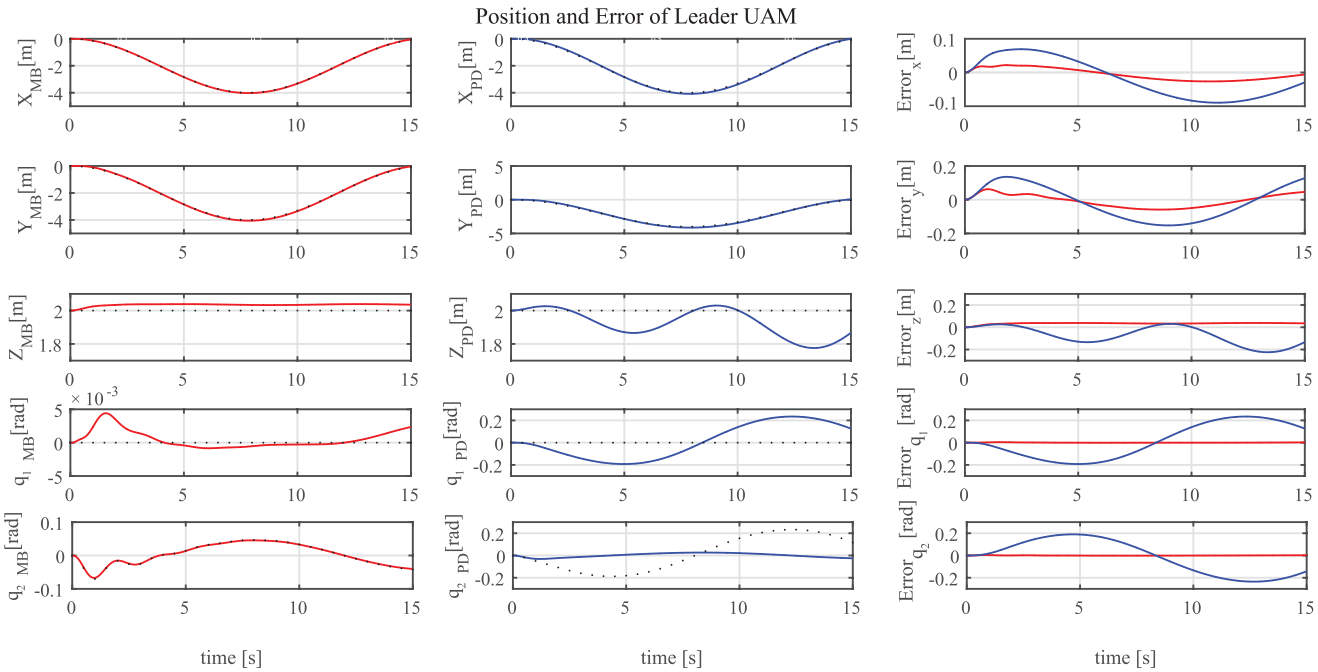

FIGURE 8. Leader UAM Controllers Comparison: The response from the model based controller is in the first column. The reference (response) trajectory is depicted in the black dotted (solid red) line. The response (solid blue) from a tuned PD controller for both the leader UAV and its manipulator is shown in the second column. In the third column, the error between the model based controller (red) and that of the PD-controller (blue) are shown.

the applied step changes in the reference trajectory, the robot leader robot compensates by adjusting its applied forces and torques, while throughout the trajectory, the applied force F_z is close to half of the object's weight 0.8×9.81 N, shared between the leader and follower UAMs.

B. SIMULATION STUDY II

The comparison of our controller against the classical non-linear tracking controller [41] embedded in the 'RotorS' simulator, followed by a PD controller for the manipulator is exemplified in Fig. 8. In this simulation study, the reference

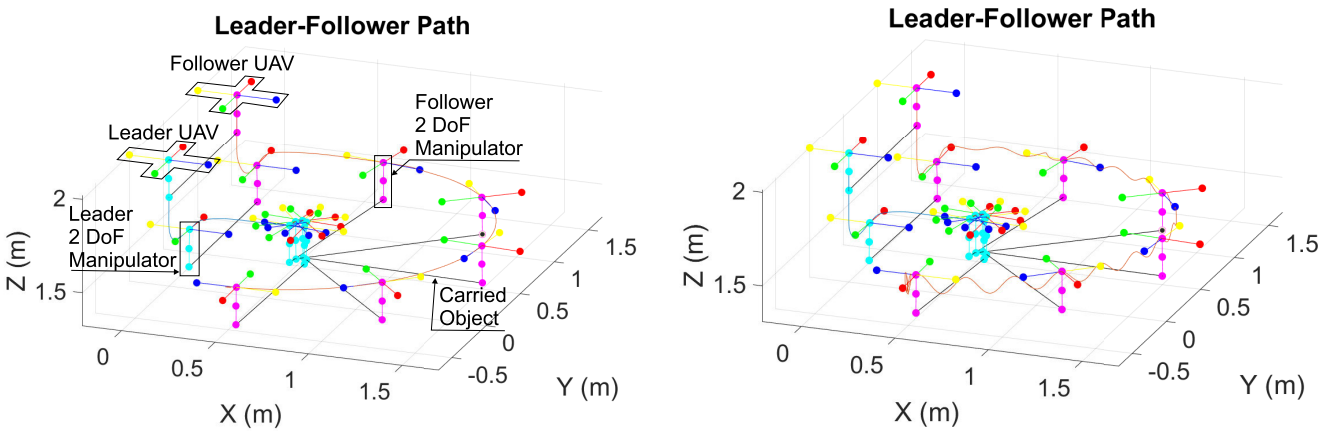

(a) $\beta = 0.2$ (b) $\beta = 2$

FIGURE 9. 3D-UAM trajectory. The leader (follower) UAM-trajectory is depicted with cyan (magenta).

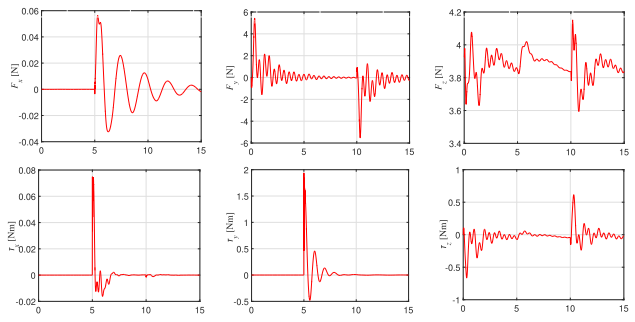

FIGURE 10. Exercised forces from the leader's manipulator.

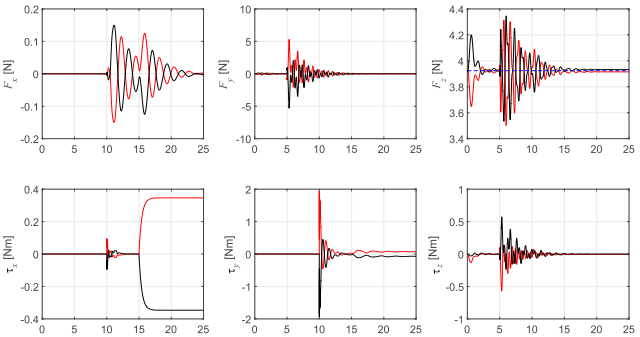

FIGURE 11. Exercised forces/torques from the leader and follower manipulators.

trajectory for the leader UAV is a sinusoidal function on X and Y axes, while maintaining its height at 2 meters. The attached manipulators have the same objectives as the previous simulation; they point perpendicular to the ground for both leader and follower while their first joint angle is perpendicular to the aerodynamic plane of pressure of the UAV. It is apparent, from the error shown in the third column, that our model based controller outperforms the suggested nonlinear PD-controller.

C. SIMULATION STUDY III

The system's response against different β-values in (21) is shown in Fig. 9, where the system exhibits oscillations for larger values of $\beta = 2$. Indirectly this amounts to an increase of the F_f-generalized force vector resulting in a larger tracking error. The UAV was asked to move from its hovering state with a 0.5 m step command (at $t = 0$) applied along the z-axis, followed by two successive 0.5 m steps along the x- and y-axes (at $t = 5$ s and $t = 10$ s), respectively. The last part of the commanded trajectory consists of a yaw command starting at $t = 15$ s, along the z-axis of the leader UAV. It should be noted that this is a rather demanding trajectory given the nature of the step inputs and the need to rotate the follower UAV around the leader one, during the yaw motion.

Fig. 11 presents the exercised torques and forces from the leader and follower manipulators, shown in red and black color respectively. During the trajectory $F_x^l \simeq -F_x^f \simeq 0$ N and $F_y^l \simeq -F_y^f \simeq 0$ N and $F_z^l + F_z^f = m_l g$ N. This is anticipated due to the maneuvers' nature and the need to have both manipulators facing downwards, with a need to carry the payload. Similarly at $t = 15$ s, there are two large opposite torques $\tau_x^l \simeq -\tau_x^f$ due to the need to have the follower rotating around the z-axis of the leader.

V. CONCLUSION

This article concerns the modeling and controlling of two UAM-systems in a leader/follower formation. Each UAM has an attached manipulator and collectively transports a load with given stiffness parameters using a suggested model

based controller. A leader/follower based controller strategy is employed. The stability of the individual tailored leader/follower controller is examined analytically. Extensive comparative simulation studies for this complicated system using the Gazebo physics engine and standard packages (Matlab) show practically no difference in the provided response, indicating the validity of the suggested model. It is shown that a model-based controller can provide satisfactory results using this leader/follower formation and outperforms classical nonlinear tracking controllers.

REFERENCES

[1] *AEROWORKS Project*. Accessed: Sep. 30, 2020. [Online]. Available: http://www.aeroworks2020.eu
[2] *ARCAS Project*. Accessed: Sep. 30, 2020. [Online]. Available: http://www.arcas-project.eu
[3] A. Ollero, J. Cortes, A. Santamaria-Navarro, M. A. T. Soto, R. Balachandran, J. Andrade-Cetto, A. Rodriguez, G. Heredia, A. Franchi, G. Antonelli, K. Kondak, A. Sanfeliu, A. Viguria, J. R. Martinez-de Dios, and F. Pierri, "The AEROARMS project: Aerial robots with advanced manipulation capabilities for inspection and maintenance," *IEEE Robot. Autom. Mag.*, vol. 25, no. 4, pp. 12–23, Dec. 2018.
[4] F. Ruggiero, V. Lippiello, and A. Ollero, "Aerial manipulation: A literature review," *IEEE Robot. Autom. Lett.*, vol. 3, no. 3, pp. 1957–1964, Jul. 2018.
[5] C. Papachristos, K. Alexis, and A. Tzes, "Efficient force exertion for aerial robotic manipulation: Exploiting the thrust-vectoring authority of a tri-tiltrotor UAV," in *Proc. IEEE Int. Conf. Robot. Autom. (ICRA)*, May 2014, pp. 4500–4505.
[6] B. B. Kocer, T. Tjahjowidodo, and G. G. L. Seet, "Model predictive UAV-tool interaction control enhanced by external forces," *Mechatronics*, vol. 58, pp. 47–57, Apr. 2019.
[7] N. Staub, M. Mohammadi, D. Bicego, Q. Delamare, H. Yang, D. Prattichizzo, P. R. Giordano, D. Lee, and A. Franchi, "The tele-MAGMaS: An aerial-ground comanipulator system," *IEEE Robot. Autom. Mag.*, vol. 25, no. 4, pp. 66–75, Dec. 2018.
[8] Y. Stergiopoulos, E. Kontouras, K. Gkountas, K. Giannousakis, and A. Tzes, "Modeling and control aspects of a UAV with an attached manipulator," in *Proc. 24th Medit. Conf. Control Autom. (MED)*, Jun. 2016, pp. 653–658.
[9] K. Gkountas, G. Ntekoumes, and A. Tzes, "Dynamics and control of an unmanned aerial vehicle employing a delta-manipulator," in *Proc. 25th Medit. Conf. Control Autom. (MED)*, Jul. 2017, pp. 1207–1212.
[10] M. Kamel, K. Alexis, and R. Siegwart, "Design and modeling of dexterous aerial manipulator," in *Proc. IEEE/RSJ Int. Conf. Intell. Robots Syst. (IROS)*, Oct. 2016, pp. 4870–4876.
[11] Z. Samadikhoshkho, S. Ghorbani, and F. Janabi-Sharifi, "Modeling and control of aerial continuum manipulation systems: A flying continuum robot paradigm," *IEEE Access*, vol. 8, pp. 176883–176894, 2020.
[12] P. E. I. Pounds, D. R. Bersak, and A. M. Dollar, "Grasping from the air: Hovering capture and load stability," in *Proc. IEEE Int. Conf. Robot. Autom.*, May 2011, pp. 2491–2498.
[13] H. Seo, S. Kim, and H. J. Kim, "Aerial grasping of cylindrical object using visual servoing based on stochastic model predictive control," in *Proc. IEEE Int. Conf. Robot. Autom. (ICRA)*, May 2017, pp. 6362–6368.
[14] C. Korpela, M. Orsag, and P. Oh, "Towards valve turning using a dual-arm aerial manipulator," in *Proc. IEEE/RSJ Int. Conf. Intell. Robots Syst.*, Sep. 2014, pp. 3411–3416.
[15] M. Tognon, B. Yuksel, G. Buondonno, and A. Franchi, "Dynamic decentralized control for protocentric aerial manipulators," in *Proc. IEEE Int. Conf. Robot. Autom. (ICRA)*, May 2017, pp. 6375–6380.
[16] G. Zhang, Y. He, B. Dai, F. Gu, L. Yang, J. Han, G. Liu, and J. Qi, "Grasp a moving target from the air: System & control of an aerial manipulator," in *Proc. IEEE Int. Conf. Robot. Autom. (ICRA)*, May 2018, pp. 1681–1687.
[17] G. Zhang, Y. He, B. Dai, F. Gu, L. Yang, J. Han, and G. Liu, "Aerial grasping of an object in the strong wind: Robust control of an aerial manipulator," *Appl. Sci.*, vol. 9, no. 11, p. 2230, May 2019.
[18] A. Suarez, A. Caballero, A. Garofano, P. J. Sanchez-Cuevas, G. Heredia, and A. Ollero, "Aerial manipulator with rolling base for inspection of pipe arrays," *IEEE Access*, vol. 8, pp. 162516–162532, 2020.
[19] A. Tagliabue, M. Kamel, S. Verling, R. Siegwart, and J. Nieto, "Collaborative transportation using MAVs via passive force control," in *Proc. IEEE Int. Conf. Robot. Autom. (ICRA)*, May 2017, pp. 5766–5773.
[20] M. Tognon, C. Gabellieri, L. Pallottino, and A. Franchi, "Aerial co-manipulation with cables: The role of internal force for equilibria, stability, and passivity," *IEEE Robot. Autom. Lett.*, vol. 3, no. 3, pp. 2577–2583, Jul. 2018.
[21] N. Michael, J. Fink, and V. Kumar, "Cooperative manipulation and transportation with aerial robots," *Auto. Robots*, vol. 30, no. 1, pp. 73–86, Jan. 2011.
[22] K. Sreenath and V. Kumar, "Dynamics, control and planning for cooperative manipulation of payloads suspended by cables from multiple quadrotor robots," in *Proc. Robot., Sci. Syst.*, Berlin, Germany, Jun. 2013.
[23] P. O. Pereira, P. Roque, and D. V. Dimarogonas, "Asymmetric collaborative bar stabilization tethered to two heterogeneous aerial vehicles," in *Proc. IEEE Int. Conf. Robot. Autom. (ICRA)*, May 2018, pp. 5247–5253.
[24] M. Bernard, K. Kondak, I. Maza, and A. Ollero, "Autonomous transportation and deployment with aerial robots for search and rescue missions," *J. Field Robot.*, vol. 28, no. 6, pp. 914–931, Nov. 2011.
[25] K. Klausen, C. Meissen, T. I. Fossen, M. Arcak, and T. A. Johansen, "Cooperative control for multirotors transporting an unknown suspended load under environmental disturbances," *IEEE Trans. Control Syst. Technol.*, vol. 28, no. 2, pp. 653–660, Mar. 2020.
[26] R. Ritz and R. D'Andrea, "Carrying a flexible payload with multiple flying vehicles," in *Proc. IEEE/RSJ Int. Conf. Intell. Robots Syst.*, Nov. 2013, pp. 3465–3471.
[27] S. Thapa, H. Bai, and J. Á. Acosta, "Cooperative aerial manipulation with decentralized adaptive force-consensus control," *J. Intell. Robotic Syst.*, vol. 97, no. 1, pp. 171–183, Jan. 2020.
[28] H.-N. Nguyen, S. Park, J. Park, and D. Lee, "A novel robotic platform for aerial manipulation using quadrotors as rotating thrust generators," *IEEE Trans. Robot.*, vol. 34, no. 2, pp. 353–369, Apr. 2018.
[29] M. Gassner, T. Cieslewski, and D. Scaramuzza, "Dynamic collaboration without communication: Vision-based cable-suspended load transport with two quadrotors," in *Proc. IEEE Int. Conf. Robot. Autom. (ICRA)*, May 2017, pp. 5196–5202.
[30] D. Mellinger, M. Shomin, N. Michael, and V. Kumar, "Cooperative grasping and transport using multiple quadrotors," in *Distributed Autonomous Robotic Systems*. Berlin, Germany: Springer, 2013, pp. 545–558.
[31] I. Maza, K. Kondak, M. Bernard, and A. Ollero, "Multi-UAV cooperation control for load transportation deployment," *J. Intell. Robotic Syst.*, vol. 57, pp. 417–449, Aug. 2010.
[32] S. Rao, A. Chakravarthy, and D. Ghose, "Planar manipulation of an object by unmanned aerial vehicles using sliding modes," *J. Guid. Control Dyn.*, vol. 44, no. 11, pp. 120–137, 2020.
[33] H. F. McCreery and M. D. Breed, "Cooperative transport in ants: A review of proximate mechanisms," *Insectes Sociaux*, vol. 61, no. 2, pp. 99–110, May 2014.
[34] K. Alexis, A. Tzes, and G. Nikolakopoulos, "Model predictive quadrotor control: Attitude, altitude and position experimental studies," *IET Control Theory Appl.*, vol. 6, no. 12, pp. 1812–1827, Aug. 2012.
[35] J. M. Hollerbach, "A recursive lagrangian formulation of maniputator dynamics and a comparative study of dynamics formulation complexity," *IEEE Trans. Syst., Man, Cybern.*, vol. 10, no. 11, pp. 730–736, Nov. 1980.
[36] M. H. Korayem and A. M. Shafei, "Motion equation of nonholonomic wheeled mobile robotic manipulator with revolute–prismatic joints using recursive gibbs–appell formulation," *Appl. Math. Model.*, vol. 39, nos. 5–6, pp. 1701–1716, Mar. 2015.
[37] K. S. Fu, R. C. González, and C. S. G. Lee, "Robotics: Control, sensing, vision, and intelligence," in *McGraw-Hill Series in CAD/CAM Robotics and Computer Vision*. New York, NY, USA: McGraw-Hill, 1987.
[38] *ODE_Simulator*. Accessed: Sep. 30, 2020. [Online]. Available: https://github.com/UPatras-ANeMoS/ode_simulator
[39] A. K. Das, R. Fierro, V. Kumar, J. P. Ostrowski, J. Spletzer, and C. J. Taylor, "A vision-based formation control framework," *IEEE Trans. Robot. Autom.*, vol. 18, no. 5, pp. 813–825, Oct. 2002.
[40] K. Gkountas, D. Chaikalis, and A. Tzes, "Force control design for a robot manipulator attached to a UAV," *IFAC-PapersOnLine*, vol. 51, no. 30, pp. 548–553, 2018.

[41] T. Lee, M. Leok, and N. H. McClamroch, "Geometric tracking control of a quadrotor UAV on SE(3)," in *Proc. 49th IEEE Conf. Decis. Control (CDC)*, Dec. 2010, pp. 5420–5425.
[42] F. Furrer, M. Burri, M. Achtelik, and R. Siegwart, "Robot operating system (ROS): The complete reference," in *RotorS—A Modular Gazebo MAV Simulator Framework*, vol. 1. Cham, Switzerland: Springer, 2016, pp. 595–625.
[43] *Asctec Pelican*. Accessed: Oct. 23, 2019. [Online]. Available: http://www.asctec.de/en/uav-uas-drones-rpas-roav/asctec-pelican

KONSTANTINOS GKOUNTAS received the integrated master's degree in electrical and computer engineering from the University of Patras (UPatras), Greece, in 2015, where he is currently pursuing the Ph.D. degree in cooperative aerial manipulation. His research interests include robotics, control systems, and system identification. He was a recipient of the Scholarship for Ph.D. studies administered by the Greek State Scholarships Foundation (IKY).

ANTHONY TZES (Senior Member, IEEE) received the degree from the University of Patras, Greece, in 1985, and the Ph.D. degree in electrical engineering from The Ohio State University, USA, in 1990.

He was the Director of the Instrumentation and Control Laboratory, Tandon School of Engineering (formerly known as Polytechnic University), New York University, from 1990 to 1999. He was the Founder and the Director of the Applied Networked Mechatronics Systems Group during his tenure at the Department of Electrical and Computer Engineering, University of Patras, from 1999 to 2016. Since 2017, he has been a Professor and the Program Head of electrical and computer engineering with New York University Abu Dhabi (NYUAD), United Arab Emirates. He is also the Director of the Robotics and Intelligent Systems Control (RISC) Laboratory, NYUAD. He has more than 85 (230) journal (conference) papers. His research interests include applied control and robotics, focusing in adaptive robust control of networked systems, and collaborative control of mobile robots and surgical robotics. He was the past Chairman of the Greek Committee at EU for the initiatives on "Coherent Development of Policies," the "Regions of Knowledge," and "Research Potential," from 2006 to 2009, and a member of the Greek Delegation of the European Control Association (EUCA) Administrative Council from 2001 to 2007. He has been on the organization committees (the Chairman, the Program Chairman, and other positions) of various international conferences and an associate editor of several journals.